Implicit and explicit host effects on excitons in pentacene derivatives

R. J. Charlton,[1,*] R. M. Fogarty,[1] S. Bogatko,[1] T. J. Zuehlsdorff,[2]
N. D. M. Hine,[3] M. Heeney,[4] A. P. Horsfield,[1] and P. D. Haynes[1]

[1]*Department of Materials, Imperial College London, Exhibition Road, London, SW7 2AZ, UK*

[2]*School of Natural Sciences, University of California Merced, 5200 N. Lake Road, Merced, CA 95343, USA*

[3]*Department of Physics, University of Warwick, Coventry CV4 7AL, UK*

[4]*Department of Chemistry, Imperial College London, Exhibition Road, London, SW7 2AZ, UK*

(Dated: May 16, 2018)

Abstract

An *ab initio* study of the effects of implicit and explicit hosts on the excited state properties of pentacene and its nitrogen-based derivatives has been performed using ground state density functional theory (DFT), time-dependent DFT and ΔSCF. We observe a significant solvatochromic redshift in the excitation energy of the lowest singlet state (S_1) of pentacene from inclusion in a *p*-terphenyl host compared to vacuum; for an explicit host consisting of six nearest neighbour *p*-terphenyls, we obtain a redshift of 65 meV while a conductor-like polarisable continuum model (CPCM) yields a 78 meV redshift. Comparison is made between the excitonic properties of pentacene and four of its nitrogen-based analogues, 1,8-, 2,9-, 5,12-, and 6,13-diazapentacene with the latter found to be the most distinct due to local distortions in the ground state electronic structure. We observe that a CPCM is insufficient to fully understand the impact of the host due to the presence of a mild charge-transfer (CT) coupling between the chromophore and neighbouring *p*-terphenyls, a phenomenon which can only be captured using an explicit model. The strength of this CT interaction increases as the nitrogens are brought closer to the central acene ring of pentacene.

* robert.charlton14@imperial.ac.uk

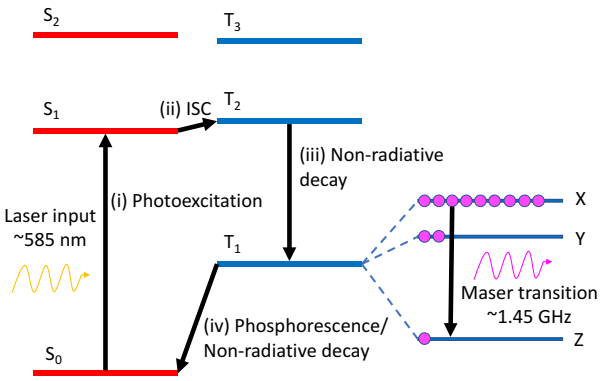

FIG. 1 – Schematic illustration of the maser mechanism using the excitation spectrum of pentacene. (i) Photoexcitation of pentacene from S_0 to S_1 using yellow light laser. (ii) Radiationless intersystem crossing (ISC) from S_1 to T_2 (see text for more details). (iii) Non-radiative decay from T_2 down to T_1, where the substates X,Y and Z are populated in the ratio 0.76:0.16:0.08, providing the necessary population inversion for the maser mechanism [**?**]. (iv) Decay from T_1 back to S_0.

I. Introduction

The sustained interest in acenes over the last decade is due to their promising electronic properties which make them suitable for organic electronic devices [**?**]. For instance, high charge-carrier mobility in the acenes, combined with their high degree of mechanical flexibility [**?**], facilitates the use of acenes and their derivatives as thin-film transistors [**? ? ?**]. Another potential application is organic photovoltaics, where pentacene and its derivatives lead the way due to the observation of singlet fission within the excitation spectrum of pentacene enabling much greater efficiency than is otherwise possible [**?**]. While the above examples are concerned with bulk crystals and thin films, the use of linear acenes as dopant materials has also been widely studied, for instance pentacene in *para*-terphenyl. One promising application of the latter system was demonstrated by Oxborrow *et al.*, who showed that a *p*-terphenyl crystal doped with pentacene can act as the gain medium for a room-temperature maser [**?**].

A simplified version of the masing mechanism in pentacene is illustrated in Figure 1.

First, the pentacene is excited by a yellow light laser from the singlet ground state S_0 to the lowest singlet excited state S_1. This singlet state is near degenerate with the triplet state T_2, giving rise to a strong mixing of these states by a combination of the spin-orbit interaction and electron-phonon interactions, thus enabling a radiationless spin-selective intersystem crossing (ISC) into the triplet state [**?**]. The matrix elements involved in this transition favour the uppermost sublevel of T_2, giving rise to a population inversion within T_2 which is preserved upon decay to the lower triplet ground state T_1, allowing masing to take place [**?**]. While this is the first successful demonstration of masing at room-temperature, further work is required before this can become a practical device, with improvements required in both efficiency and enabling continuous operation of the maser [**?** **?**]. One major constraint is the slow rate of decay from T_1 back to S_0, resulting in a build-up of excitons in the lowest triplet state which suppresses the population inversion in T_1.

Given its role in enabling the first working room-temperature maser, pentacene has acted as the prototype for further experimental and theoretical research into potential maser active molecule candidates which may bring improvements in performance. One possibility would be to replace pentacene with its nitrogen-based analogues, some examples of which are shown in Figure 2. Experimental studies comparing anthracene to its analogue phenazine, in which the central aromatic ring contains two sp^2 nitrogen groups, find that the zero field splitting is comparable but there is a much more pronounced population inversion for phenazine, resulting in strong phosphorescence [**?**]. An equivalent effect for a pentacene derivative would result in a faster ISC in the pentacene in *p*-terphenyl maser.

It is known experimentally that the pentacene excitation spectrum can vary significantly depending on the host in which the pentacene resides [**?** **?** **?**]. For instance, Heinecke *et al.* demonstrated by laser spectroscopy that the lowest singlet excitation S_1 is found at 2.31 eV for gas phase pentacene, but experiments on pentacene in *p*-terphenyl show results of 2.1 eV [**?**]. The potential impact of this difference on the ISC rate is very significant – Patterson *et al.* observed an increase in the rates by two orders of magnitude from a shift of 20 meV, corresponding to the pentacene being located in one of four different lattice sites in the *p*-terphenyl herringbone structure, each of which yields a distinct feature in the absorption spectrum [**?**]. An *ab initio* description of the pentacene in *p*-terphenyl maser

must therefore be able to capture not just the vacuum excitation energies of pentacene, but also the impact of the host.

First principles calculations of the excitonic properties of pentacene are usually performed in vacuum or bulk pentacene, rather than in doped molecular structures. Bogatko *et al.* have performed an *ab initio* study using time-dependent density functional theory (TDDFT) [**?**] in order to screen possible active molecules from among the linear acenes [**?**], comparing properties such as the $|S_1 - T_n|$ energy splitting in these molecules to provide a qualitative comparison with pentacene. Much work has gone into understanding from first-principles the impact of charge-transfer (CT) excitons on the excited state properties of acenes in the context of Davydov splitting [**?** **?**] as well as the importance of charge delocalisation via explicit quantum mechanical descriptions compared with embedded charge models [**?**]. Such studies focus on clusters in crystalline acene structures, rather than doped molecular crystals such as pentacene in *p*-terphenyl.

Solvent environments can be simulated implicitly by the inclusion of a dielectric medium but, as Bogatko *et al.* found with their TDDFT study, the impact this has upon the excitation spectrum is limited [**?**]. More detailed explicit solvent simulations have been restricted by the computational cost involved in explicit quantum mechanical approaches to such systems, which can extend to include thousands of atoms. Indeed, the limits of wave function-based quantum chemical methods are already being pushed by pentacene alone, so any explicit inclusion of the environment with such approaches is currently impossible [**?**]. Past studies have sought to identify the importance of including explicit solvent regions in quantum mechanical calculations when performing QM/MM style calculations with implicit solvent and polarisable continuum model (PCM). In these studies, shells of water molecules were included in the quantum mechanical region, yielding shifts in the excitation spectra depending on the environment and indicating that an explicit description of at least nearest neighbour molecules is required to accurately capture solvent effects [**?** **?** **?**].

In this paper, we present a first principles study of the ground and excited state properties of pentacene in an explicit *p*-terphenyl host. We make use of linear-scaling DFT as implemented in the ONETEP package [**?**] for ground state properties and we compare the excitonic properties of pentacene in implicit and explicit hosts using semi-local

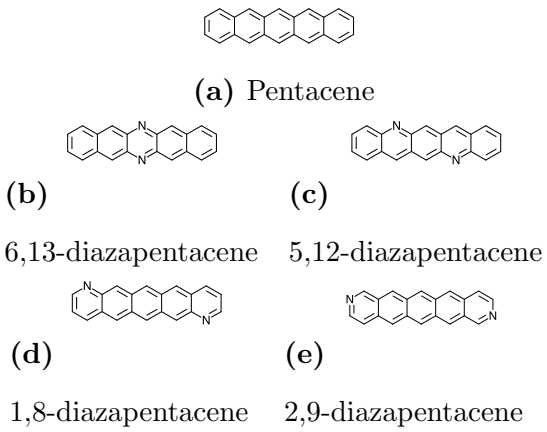

FIG. 2 – Dopant molecules considered as part of this study. For brevity, each diazapentacene molecule will be referred to by the shorthand "m,n-dap" throughout this work.

and optimally-tuned range-separated hybrid exchange-correlation functionals in Gaussian 09 [**?**]. We extend this approach to compare the behaviour of pentacene to a selection of its nitrogen-based analogues, displayed in Figure 2, as previously studied by Bogatko *et al.* Finally, we discuss the electronic structures of these acenes, their interaction with the host environment and the implications that these phenomena have for the maser and similar systems.

II. Ground state methods – Linear-scaling DFT

Kohn-Sham density functional theory (KS-DFT) [**?** **?**] has become a popular method due to its balance between accuracy and computational efficiency when compared with other electronic structure methods. Standard implementations of KS-DFT have a computational cost that scales cubically with system size [**?**]. While this is very good compared to other quantum chemical methods, it renders larger systems consisting of thousands of atoms, such as the *p*-terphenyl crystal studied as part of this work, beyond the limits of conventional DFT codes. One approach to avoid this unfavourable scaling is to treat the single-particle density matrix as the fundamental quantity, rather than the charge density. This allows one

to exploit the nearsightedness of electronic structure for insulators [**?** **?**], which reduces the theoretical cost of the problem to linear scaling [**?**]. In this work, we make use of linear-scaling DFT as implemented in the ONETEP package [**?**]. In ONETEP the density matrix is expanded in terms of a set of localised atom-centred orbitals $\{\phi_\alpha\}$, referred to as non-orthogonal generalised Wannier functions (NGWFs) [**?**], such that

$$\rho\left(\mathbf{r},\mathbf{r}'\right)=\sum_{\alpha,\beta}\phi_\alpha\left(\mathbf{r}\right)K^{\alpha\beta}\phi_\beta\left(\mathbf{r}'\right), \tag{1}$$

where $\mathbf{K}$ is the density kernel, a generalisation of the Kohn-Sham orbital occupancies that, if sparse, yields linear-scaling. Convergence of the total energy is performed in two nested loops, whereby the elements of $\mathbf{K}$ and the NGWFs are iteratively adapted in sequence until self-consistency is achieved. The accuracy of the NGWF basis is controlled by two parameters: the NGWF radius, outside of which the NGWFs are zero, and the kinetic energy cutoff, which sets the spacing for the grid upon which the NGWFs are expanded. Using this basis enables us to perform calculations with linear-scaling effort that are systematically improvable to plane wave accuracy [**?**].

A. Chromophores and the crystal host

All geometry optimisations were performed in ONETEP using the PBE exchange-correlation functional [**?** **?**]. Our crystal host was generated by constructing a *p*-terphenyl crystal in a $3\times4\times3$ periodic cell of 72 *p*-terphenyl molecules with atomic positions and lattice parameters taken from experiment [**?**]. At room temperature, *p*-terphenyl has a crystal structure with just two distinct lattice positions. A pentacene molecule was substituted in place of a single *p*-terphenyl in this structure, maintaining the same orientation and centre of mass. This is in keeping with the experimentally observed pentacene in *p*-terphenyl structure, where the pentacene occupies a region of similar size to the *p*-terphenyl it replaces. Due to the lack of dispersion in PBE, we did not perform a full geometry optimisation of the crystal at this point. Instead, the pentacene geometry was reoptimised while holding the *p*-terphenyl carbon atoms fixed so as to maintain the experimentally observed structure – all host hydrogens were also reoptimised. The resulting structure was used for all our

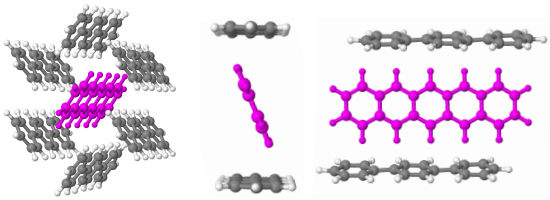

(a) **(b)** **(c)**

FIG. 3 – (a) Arrangement of the pentacene (centre, pink) and the six nearest neighbour *p*-terphenyls for cluster calculations. (b) Orientation of pentacene within the herringbone structure. A transformation of pentacene via reflection through its major axis would show the alternative lattice position. (c) Alignment of the acene rings within pentacene and *p*-terphenyl.

subsequent work – see the Supplementary Material (SM) for more details.

Four alternative dopant molecules were considered based on the previous work of Bogatko *et al.* [**?**] by substituting nitrogen for carbon in the pentacene to generate the molecules shown in Figure 2. The geometries were subsequently reoptimised using the same procedure as for pentacene. We did not investigate any of the other linear acenes considered by Bogatko *et al.* as, due to the significant difference in their size from pentacene, they would not fit comfortably within the *p*-terphenyl crystal. The choice of an appropriate host for these alternative molecules remains an open question both theoretically and experimentally.

For excited state properties discussed later, we extracted a cluster of pentacene and its six nearest neighbour *p*-terphenyls from the periodic crystal as shown in Figure 3. This acted as the explicit host for the subsequent excited state calculations. The cluster was selected by analysis of the HOMO and LUMO states of pentacene in the periodic crystal – inclusion of an explicit host results in a non-zero contribution from neighbouring *p*-terphenyls to these orbitals with semi-local functionals. We selected the cluster of six *p*-terphenyls to ensure that these states could be fully captured by the pentacene and its neighbouring molecules – see SM for more details. A conductor-like polarisable continuum model (CPCM) was also used as the implicit solvation model for comparison with explicit host results.

III. Excited state methods

In this work we have used two methods to calculate excited state energies – time-dependent density functional theory (TDDFT) and ΔSCF, the latter for the T_1 state for comparison with TDDFT results. As T_1 is the ground state of the system with electron spin in a triplet state, it can be studied reliably using ground state DFT.

A. TDDFT and the conjugated states

It is well known that TDDFT implementations that utilise semi-local exchange-correlation functionals have problems describing the excited states of linear acenes [**?** **?** **?**]. Singlet excitation energies in particular are significantly underestimated due to the failures to describe the π-conjugated states of pentacene. This precludes using semi-local functionals in direct comparison to experimental results or more accurate first principles approaches for absolute energies which have been explored elsewhere for vacuum pentacene [**?**]. Instead, we will focus on comparing PBE vacuum results with similar calculations using hybrid functionals, which will enable us to evaluate whether trends in molecular behaviour between pentacene and its derivatives are dependent on the functional used.

For environment comparisons, it is necessary to determine whether the distortion of excitation energies by semi-local functionals is systematic in nature and thus whether trends between different functionals can be rigorously compared. In particular, the use of semi-local exchange-correlation functionals with TDDFT does not give a good representation of long-range interactions, resulting in long-range charge-transfer (CT) states being unphysically low in energy. Figure 4 gives a graphical demonstration of this issue for pentacene in a *p*-terphenyl environment. The physical, localised pentacene excited states have become mixed with CT states from the host system, requiring the calculation of a large number of states in order to obtain the pentacene spectrum. This is problematic as the cost of calculating the excitation spectrum with linear-response TDDFT scales as $O\left(N_\omega^2\right)$, where N_ω is the number of excited states, rendering higher energy excited states beyond the reach of this method. The presence of these CT states can thus make it difficult to probe the localised pentacene

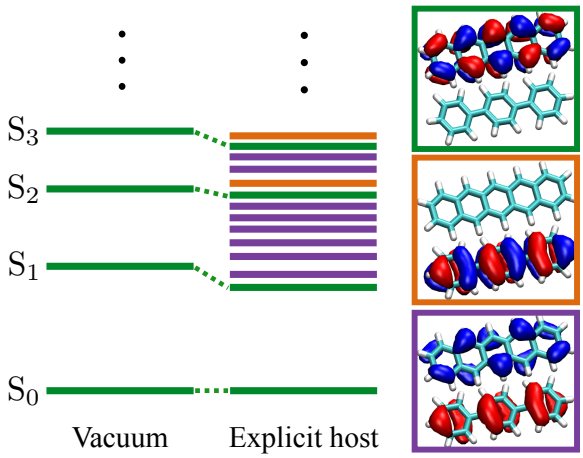

FIG. 4 – Schematic representation of the TDDFT excitation spectrum of pentacene in an explicit *p*-terphenyl host compared to the vacuum equivalent using a semi-local exchange-correlation functional. The figures on the right depict the electron (blue) and hole (red) densities of the excitations for a pentacene and *p*-terphenyl system. From top to bottom: pentacene excited state (green), *p*-terphenyl excited state (orange), charge-transfer state (purple). The green pentacene states are shifted in energy by the influence of the host.

states in a host structure.

One approach to remove these spurious CT states is the kernel truncation strategy employed by Zuehlsdorff *et al.* [**?**]. In that work, excited states composed of Kohn-Sham transitions between the chromophore and shells of explicit solvent were forbidden outside of a specified radius. Although we did attempt to use this for our system, we found that the impact of this truncation on the excitation energies was too severe to be of use for this system, thus the results are not presented here. Further information can be found in the SM.

B. Optimally tuned range-separated hybrid functionals

Hybrid functionals that include a portion of exact exchange give a more realistic description of these CT states by correcting the self-interaction error associated with semi-local functionals, thus removing them from the low-lying spectrum. In particular, the use of optimally tuned (OT) range-separated hybrid functionals has previously led to accurately calculated excitation energies even in cases which are difficult for TDDFT, including the acene series and CT excitations [**?** **?** **?**]. For this reason, we employ the OT-LCωPBE functional alongside PBE for excited states. The OT-LCωPBE functional has the same form as the standard LC-ωPBE functional, with 100% semi-local exchange at short range and 100% exact exchange at long range [**?**]. The range separation parameter is tuned such that the calculated ionisation energy matches the negative of the highest occupied molecular orbital (HOMO) eigenvalue ϵ_{H}; this is a property of the exact (unknown) Kohn-Sham DFT functional and hence this tuning procedure is physically motivated [**?**]. The calculated ionisation energy is determined as the difference in energies from an SCF calculation on the neutral and ionised species, such that the tuning criterion is $E_{N-1} - E_N = -\epsilon_{\mathrm{H}}$, where N is the number of electrons in the system.

IV. Calculation specifications

All ONETEP calculations presented here have been performed using a kinetic energy cutoff of 750 eV and the PBE exchange-correlation functional for ground state DFT calculations. For valence states, the NGWF radius was fixed at 10 bohr, while conduction state NGWFs had a radius of 15 bohr [**?**]. In both cases the number of NGWFs centred on each atom was chosen as 1 per H, 4 per C and 4 per N [**?**].

All Gaussian 09 calculations were carried out with the cc-pVTZ basis set [**?**] at geometries obtained from ONETEP calculations. The numerical integration grid was tightened from the defaults to a pruned grid with 99 radial shells and 590 angular points per shell. For CPCM calculations, both the static and optical dielectric constants were set to 3; a single

TABLE I – Experimental and selected *ab initio* data from this study and the literature for lowest pentacene excitations in vacuum.

	S_1 (eV)	T_1 (eV)
Experiment [**?**]	2.3	0.86
Multi-reference Møller-Plesset perturbation theory (MRMP) [**?**]	2.31	0.87
CCSD(T) (vertical excitation) [**?**]	-	1.37
PBE TDDFT	1.62	0.81
OT-LCωPBE TDDFT	2.15	0.58
PBE ΔSCF	-	0.91
OT-LCωPBE ΔSCF	-	1.08

value was used due to the similarity between the dielectric constant of *p*-terphenyl in the microwave spectrum (2.98) and at optical frequencies (2.81) [**?** **?**].

Excited state calculations were performed using both TDDFT and ΔSCF in Gaussian 09 [**?**]. For ΔSCF, single point calculations were performed in both the singlet and triplet ground states S_0 and T_1 respectively. In both cases the S_0 geometry was used, corresponding to vertical excitation energies. TDDFT and ΔSCF calculations in ONETEP were also performed and are reported in the SM [**?**]. No corrections were employed to account for the Stokes shift that would result from relaxation of the molecular geometry into the excited state configuration.

Population analysis was performed using the natural bond orbital (NBO) method [**?**] as implemented within the GENNBO package [**?**] and interfaced with ONETEP [**?**]. Density of states (DOS) plots were generated using Gaussian functions with a full width at half-maximum of 0.2 eV. For the local DOS (LDOS), the area for each Gaussian was set to the fractional contribution determined using Multiwfn 3.4.2 [**?**].

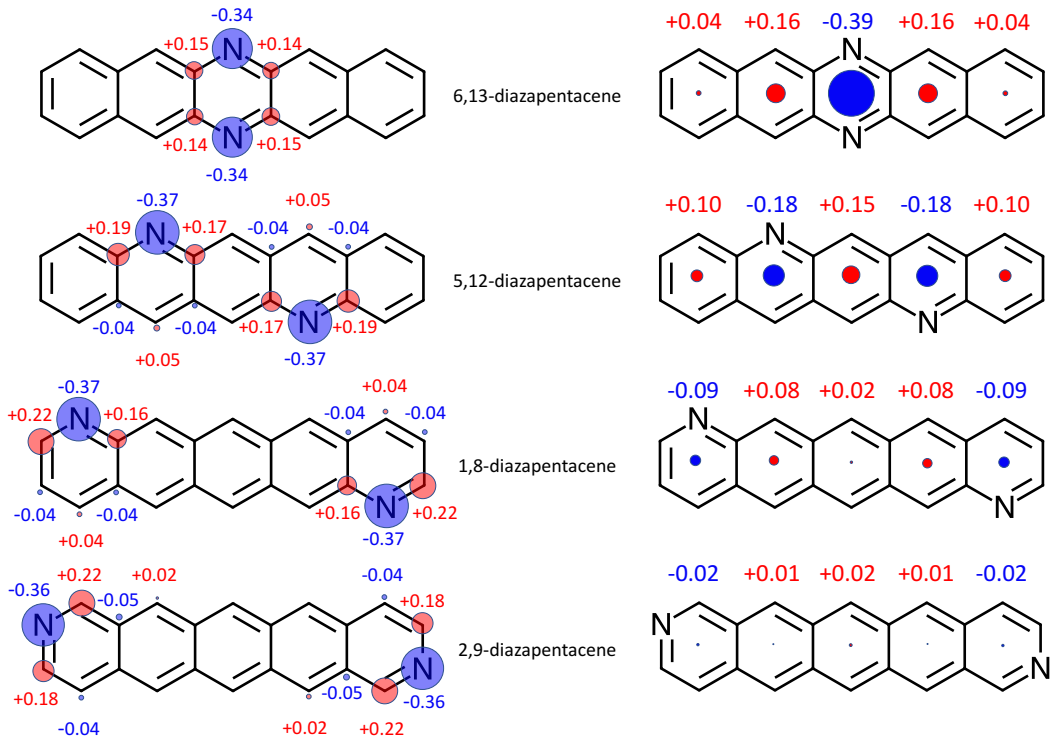

FIG. 5 – Natural bond orbital (NBO) analysis of populations for each atom (left) and acene ring (right) with respect to pentacene. For nitrogens, results are compared to the total electron population of the corresponding C-H bond. The radius of each circle is proportional to the net electron population displayed. Atoms with charge variation of ±0.01e or lower are omitted.

V. Vacuum results

A. Ground state electronic properties

Before we begin our study of the excitonic properties of the chromophores, it is useful to consider the ground state electronic structure of the various molecules and, in particular, what impact the presence of the nitrogens has compared to pentacene. Figure 5 shows the population on each atom within each chromophore with respect to pentacene using natural bond orbital (NBO) analysis [**?**]. Due to the higher electronegativity of nitrogen

compared to carbon, we see a significant accumulation of negative charge at the nitrogen sites with corresponding decreases in the electric charge of neighbouring carbon atoms or C-H structures. This is consistent with past studies of the impact of nitrogen substitution on pentacene dimers [**?**] and π-π interactions in benzene and pyridine [**?**], whereby charge redistribution across the acene structure results in a mild electric dipole and the spatial extent of the π-electron density is reduced.

Chemically, the central acene ring of pentacene is more reactive than the outer rings due to variations in the charge density. Applying our NBO analysis to the rings of pentacene, we observe a small redistribution of charge across the molecule; the three central rings possess a net charge of -0.004e while the outer rings possess a net +0.006e charge. Figure 5 also displays the change in acene ring populations with respect to pentacene for each molecule. 6,13-diazapentacene (dap) shows a significant net accumulation of -0.39e charge on the central ring, with a smaller change of +0.16e for the neighbouring rings. A similar but less striking effect is observed for 5,12-dap, with significant variations of charge on each ring though the effect is more balanced than for 6,13-dap. By contrast, 1,8-dap and 2,9-dap reveal little change in the electronic properties of each ring; indeed, 2,9-dap shows virtually no change at all compared to pentacene as all the charge collected by the nitrogens come from the same ring due to its unique location, thus the net change on each ring is effectively neutral. Similarly for 1,8-dap, the nitrogens are located on the outermost rings, such that charge is being absorbed from other atoms on this ring, resulting in a small net change in the charge across these rings with respect to pentacene. This phenomenon can be seen by examining the atomic populations in Figure 5, where the only appreciable change in population takes place on the same rings as the nitrogens occupy, implying that this is a highly localised effect. Even so, the charge variations within all our chromophores are significantly greater than the pentacene results mentioned above. Our ground state analysis thus implies that 1,8- and 2,9-dap maintain a predominantly acene-like character, whereas the electronic structure of 6,13-dap has been substantially distorted, making it distinct from pentacene.

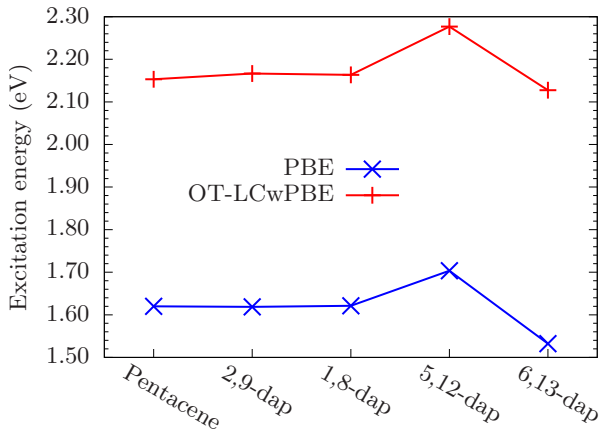

FIG. 6 – Comparison of S_1 energy for each chromophore in vacuum with TDDFT using PBE and OT-LCωPBE exchange-correlation functionals.

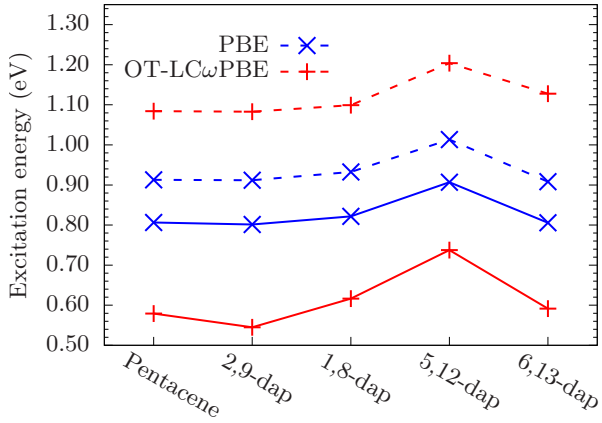

FIG. 7 – Comparison of T_1 energy for each chromophore in vacuum with TDDFT and ΔSCF calculations. Solid lines use the same key as Figure 6 for TDDFT data. Broken lines represent ΔSCF results.

B. Vacuum excitations

Next, we consider the excited state properties of our chromophores in vacuum. This will form the reference for our study of the environment effects on the acenes. Figures 6 and 7 show the vacuum energy levels of S_1 and T_1 for all five molecules outlined in Figure 2 using

TDDFT and ΔSCF in Gaussian. We see that PBE behaves consistently for S_1 and T_1, with the same trends between molecules observed regardless of method or exchange-correlation functional. As expected from our discussion in Section III A, the absolute PBE S_1 energies are considerably lower than experimental and quantum chemical results presented in Table I. Hybrid functionals perform much better for S_1, while for T_1 with TDDFT we observe a significant underestimation of the energy level using hybrid functionals, where PBE gives a considerably better result. This is most likely a result of the triplet instability associated with linear-response TDDFT [**?** **?** **?**]. For comparison, we include ΔSCF results using each functional. The closest results to experiment for the T_1 state of pentacene are obtained using PBE, as hybrid functionals now appear to overestimate the excitation energy. Nonetheless, the hybrid result is in line with past first principles calculations of T_1 with high-level methods [**?**]. Once again we observe the same trends regardless of functional and method, indicating that the variation in excitonic properties caused by nitrogen doping can be captured by PBE without requiring exact exchange, even if the absolute energies are underestimated, but the use of full TDDFT can lead to poor results with hybrid functionals. Further consistency tests have been performed using the Tamm-Dancoff Approximation (TDA) and other exchange-correlation functionals which confirm the observations discussed here. In particular, using the TDA yields results in agreement with ΔSCF. Details are included in the SM.

VI. Host effects

We now consider the impact of placing our molecules in both implicit and explicit *p*-terphenyl hosts, the former a conductor-like polarisable continuum model (CPCM) and the latter a cluster of six *p*-terphenyls as shown in Figure 3. Our focus is on the trends that we observe by comparing these results to the vacuum results outlined in Section V B. Due to the close agreement between TDDFT with OT-LCωPBE and past studies for S_1, as well as ΔSCF and TDA, from here on all S_1 energies will be calculated using TDDFT and T_1 energies with ΔSCF.

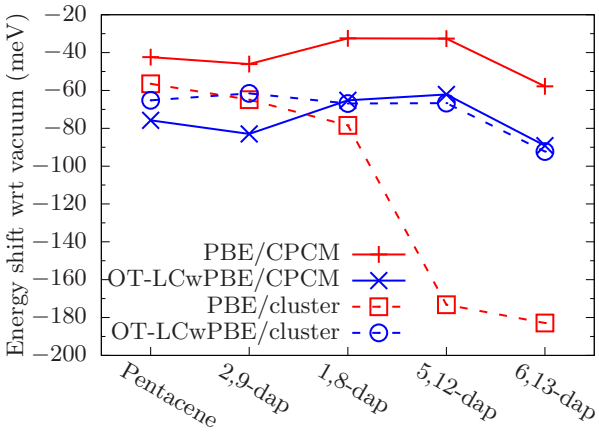

FIG. 8 – Change in S_1 energy level for each chromophore by insertion into a CPCM (solid lines) and explicit host of 6 *p*-terphenyls (dashed lines) compared to vacuum with PBE (red) and OT-LCωPBE (blue). All calculations were performed with TDDFT. This figure uses the same legend as Figure 9.

A. Results

Figure 8 displays our results for the S_1 excitation energies of all our chromophores in both implicit and explict host with PBE and OT-LCωPBE. Starting with the CPCM, we see a redshift in S_1 for all molecules, though for PBE the magnitude of the redshift is 30-40 meV smaller than the OT-LCωPBE result. Both functionals predict the same trend between different chromophores, with 2,9- and 6,13-dap showing a greater redshift than pentacene, while the solvatochromic shift is reduced for 1,8- and 5,12-dap. With an explicit host, we observe significant divergence between PBE and OT-LCωPBE. While there is a greater redshift for OT-LCωPBE than PBE for pentacene, this trend is reversed for the other chromophores and appears to be magnified as the nitrogens are brought closer together, with PBE predicting a greater redshift for all nitrogen-based analogues than the hybrid functional. Indeed, the S_1 PBE results for 5,12- and 6,13-dap in explicit host predict redshifts of 173 meV and 189 meV respectively, far greater than any other shift presented here. With OT-LCωPBE, pentacene is redshifted by 65 meV, a result comparable to those for all other chromophores apart from 6,13-dap, for which we see a greater shift of 92 meV.

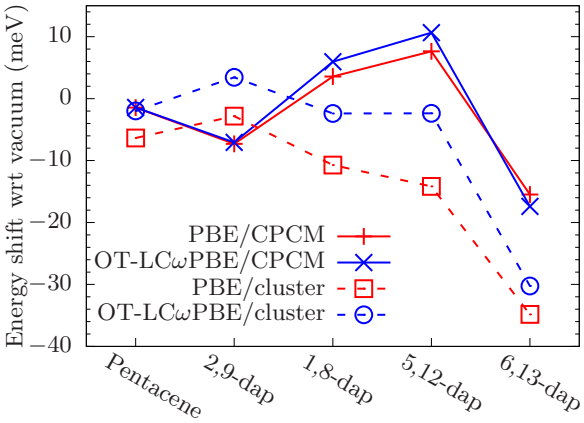

FIG. 9 – Change in T_1 energy level for each chromophore by insertion into a CPCM (solid lines) and explicit host of 6 *p*-terphenyls (dashed lines) compared to vacuum with PBE (red) and OT-LCωPBE (blue). All calculations were performed with ΔSCF.

Turning our attention to T_1, Figure 9 shows the equivalent results for the lowest triplet state using ΔSCF, the scale of which are considerably smaller than S_1. Looking at the CPCM results, we notice that near-zero redshifts are predicted for pentacene with both the PBE and OT-LCωPBE functionals, which amounts to just 2 meV. We observe the same trends between chromophores for both functionals as well, with the magnitude of the solvatochromic shift being significantly reduced compared to S_1. Indeed, 1,8- and 2,9-dap have small blueshifts of 6 meV and 11 meV respectively compared to vacuum, with only 6,13-dap predicting a significant redshift of 15-18 meV. With the cluster, we see that both PBE and OT-LCωPBE predict the same trends between the chromophores, though the latter predicts a smaller redshift in all cases; indeed, for 2,9-dap OT-LCωPBE produces a blueshift, though since the shift is below 5 meV this may not be an significant result. As with the CPCM, 6,13-dap sees the most significant change, being redshifted by 30-35 meV relative to vacuum.

B. Discussion

At this stage, we must try to unravel the effects of the choice of exchange-correlation functional and host medium on the excited state properties of our oligoacenes. The stand-

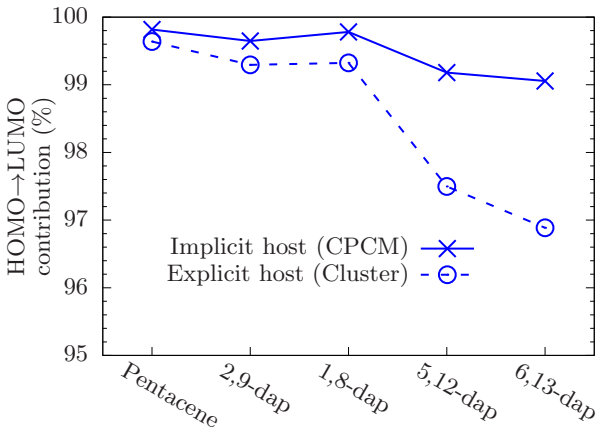

FIG. 10 – Contribution of the HOMO→LUMO Kohn-Sham transition vector to the S_1 excited state of the chromophores in implicit and explicit *p*-terphenyl host using OT-LCωPBE.

out data from Figures 8 and 9 is the shift in S_1 for 5,12- and 6,13-dap using PBE, results which are distinct from all the others presented here. A closer look at the composition of the S_1 state for each molecule reveals the reason for this. While in vacuum this transition is entirely HOMO→LUMO in character, for explicit host we see a mixing of other charge-transfer (CT) transitions between the chromophore and *p*-terphenyl into the S_1 excitation for these molecules, with the HOMO→LUMO transition contributing only 56% and 66% to S_1 for 5,12- and 6,13-dap respectively. By comparison, the S_1 states for pentacene, 2,9-dap and 1,8-dap possess a 97%, 95% and 94% HOMO→LUMO contribution respectively – see SM for more details. Figure 10 shows the equivalent results using OT-LCωPBE, where the HOMO→LUMO transition dominates for all molecules. It thus appears that this spurious CT mixing caused by the failure of PBE to capture long-range interactions has resulted in an unphysically large redshift for S_1. We do not observe the same phenomenon for T_1 since this state retains its highly localised Frenkel excitonic state in all oligoacenes.

Comparing the energetic trends for CPCM and explicit host, we notice near identical behaviour for 1,8-, 5,12- and 6,13-dap using OT-LCωPBE for S_1, while the two models diverge for pentacene and especially 2,9-dap. Note that, in contrast to the explicit host, we observe qualitatively similar behaviour with a CPCM using both functionals, although PBE

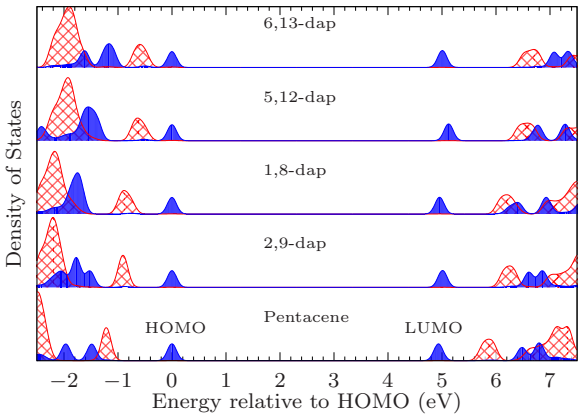

FIG. 11 – Local density of states (LDOS) of the different chromophores in explicit host as a function of energy with OT-LCωPBE. Blue/solid: acene LDOS. Red/patterned: *p*-terphenyl cluster LDOS. Energies are relative to the HOMO of the given chromophore in explicit host.

underestimates the magnitude of the redshift in S_1 that OT-LCωPBE predicts. Comparing functionals alone, however, masks the impact of the nitrogen doping on S_1, as the CPCM predicts a smaller redshift for 1,8- and 5,12-dap than pentacene, in contrast to the explicit host results, as well as underestimating the scale of the shift for 6,13-dap relative to pentacene. This becomes clearer form Figure 9, where the two models predict markedly different trends despite producing identical results for pentacene with OT-LCωPBE. This indicates that, while the CPCM does provide a good description of the impact of the electrostatic interaction on between pentacene and the *p*-terphenyl host, it fails to capture the full impact of the environment interactions on the nitrogen doped molecules.

Figure 10 compares the contribution of the HOMO→LUMO transition to S_1 for both implicit and explicit hosts using OT-LCωPBE. While in vacuum this is a pure HOMO→LUMO transition, we observe a small but significant dilution of this excited state from inclusion of an explicit host, the magnitude of which increases as the nitrogens are brought closer together within the acene. Note that this is qualitatively similar to our observations for PBE, even though the scale of the dilution is vastly overestimated by semi-local functionals. The CPCM is unable to capture this CT contribution to the excited state, leading to the difference between the solvatochromic shifts observed in the two models. To understand how this

is related to nitrogen doping, consider the local density of states (LDOS) plots displayed in Figure 11. While in vacuum pentacene the HOMO and LUMO are isolated energetically, the inclusion of an explicit host introduces additional molecular orbitals above the vacuum HOMO-1 and below the LUMO+1. The HOMO/LUMO states of pentacene in *p*-terphenyl retain their purity but nitrogen doping brings the occupied states of the host molecules closer to the HOMO in energy. Our calculations show that the nitrogen lone pairs provide a bridging mechanism between the pentacene molecular orbitals and those of *p*-terphenyl, rendering these states available for inclusion as weak CT contributions to the oligoacene excited states.

Hohenstein and Sherrill have shown the importance of the substitution of nitrogen heteroatoms in π-π interactions using the example of benzene and pyridine dimers [**?**]. The highly electronegative nitrogens reduce the spatial reach of the electron density, resulting in a stronger bond with benzene due to the orientation of this nitrogen with the net-positively charged hydrogen on the benzene molecule. A similar mechanism can be expected for the doping of pentacene with nitrogen, as from Figure 3b we see that there will be a high degree of overlap between the pentacene and *p*-terphenyl rings in the herringbone structure. As we have just seen, however, the strength of the CT coupling resulting from this interaction varies significantly for our oligoacenes, with pentacene, 1,8- and 2,9-dap showing near identical singlet and triplet excitation energies in vacuum and explicit host, while 5,12- and 6,13-dap are more distinct. This is consistent with our observation in Section V A that the latter two molecules show a significant redistribution of their electron charge due to the introduction of the nitrogen lone pairs into the aromatic system, while the former are almost indistinguishable from pentacene. Since 1,8- and 2,9-dap retain a predominantly acene-like character, their excitonic behaviour resembles that of pentacene, unlike 5,12- and 6,13-dap.

From a geometric perspective, Figure 3 shows clear differences between the regions that each nitrogen lone pair interacts with on neighbouring *p*-terphenyls. In addition, from Figure 2, we see that, apart from 6,13-dap, all diazapentacene molecules lack the mirror symmetry through the major axis plane that pentacene possesses. We thus considered rotating all the molecules to give the alternative lattice position in the *p*-terphenyl crystal, with the view that this may affect the lone pair interactions. However, we observed no appreciable change

in excitation energies or molecular orbital composition for any molecule, which appears to rule out this geometric theory. We therefore conclude that the unique excitonic properties of 6,13-dap can be attributed to the strong distortion of the local electronic structure by the presence of the nitrogens.

VII. Conclusions

In this paper, we have presented a first-principles study of the excitonic properties of pentacene and its nitrogen based analogues doped in both implicit and explicit *p*-terphenyl hosts. We have demonstrated, using both ground-state DFT and TDDFT, that the presence of a host has significant effects upon the S_1 excitation energy of the chromophore. Implicit solvation is often insufficient to understand host effects, requiring one to employ explicit treatments of the host in regions neighbouring the chromophore due to a weak charge-transfer interaction between the guest dopant and neighbouring *p*-terphenyls. However, an implicit model does provide a qualitative understanding of the importance of the environment for treating excited excited states of these oligoacenes from an electrostatic perspective. For instance, our CPCM predicted a significantly stronger redshift in the lowest triplet state T_1 for 6,13-diazapentacene than the other chromophores which, though it does not match the explicit results, indicates that these oligoacenes have quantitatively different behaviours in host systems. Even with semi-local functionals, it is possible to obtain indicative trends of environment behaviour of these chromophores that match hybrid treatments as in CPCM the spurious charge-transfer mixing is not a factor. This, however, hides the failure of semi-local functionals with explicit host and highlights that explicit host models with hybrid exchange-correlation functionals are the combination required to obtain reliable results for the full impact of the environment in such systems.

From the perspective of the search for new chromophores for the room-temperature maser, our study shows that significant variations in the excited states of these molecules can result from the presence of nitrogen in the molecule due to the highly electronegative behaviour of the nitrogen atoms causing charge redistribution across the molecules. This facilitates a stronger interaction with the *p*-terphenyl host for 6,13-dap than the other chromophores,

resulting in a greater redshift of the low-lying excited states. For 1,8- and 2,9-dap, the effect of charge redistribution is localised on the outer rings, thus the variation in electric charge across the rings is significantly reduced and the impact on excitation delocalisation is minimal. These molecules thus have excitation spectra that are very similar to pentacene, suggesting that they could be functional maser media dopant molecules. 5,12-dap behaves similarly to pentacene in response to the *p*-terphenyl host, but T_1 is significantly higher than for any other molecule studied here, which would have a detrimental effect on the decay rate from T_1 back to S_0. 6,13-dap sees a significant distortion of the excitation spectrum, due to the presence of the nitrogens on the central acene ring, as well as a greater redshift in a *p*-terphenyl host than for pentacene. The significant redshift of T_1 could aid the decay rate and avert bottlenecking that affects the current device. The use of nitrogen substitution enables one to largely preserve the excitation spectrum of pentacene while tuning the interaction between the chromophore and its host, thus understanding the interactions between such molecules and their hosts is essential for such techniques to be used in practical applications.

Supplementary Material

See the Supplementary Material for additional information on geometry optimisations and how the cluster was constructed, as well as additional excitation energy plots using the Tamm-Dancoff approximation (TDA) and other exchange-correlation functionals. The research data from this publication is freely available at https://doi.org/10.5281/zenodo.1167847.

Acknowledgments

The authors wish to thank Dr Mark Oxborrow and Dr Jess Wade for useful discussions. The authors acknowledge support from the Thomas Young Centre under grant TYC-101. RJC acknowledges studentship support from the EPSRC Centre for Doctoral Training Centre in Theory and Simulation of Materials (EP/L015579/1) and an Imperial College Presidents PhD Scholarship. PDH acknowledges support from the Engineering and Physical Sciences Research Council (EPSRC) Platform Grant EP/J015059/1. APH, PDH, SB and RMF

acknowledge funding by the Leverhulme Trust under Research Project Grant RPG-2014-125. NDMH and PDH acknowledge support from the Engineering and Physical Sciences Research Council (EPSRC) Grant EP/P02209X/1. Calculations were performed at the Imperial College Research Computing Service, doi:10.14469/hpc/2232.